

High-gain, free-electron laser amplifiers: Design considerations and simulation

D. Prosnitz, A. Szoke, and V. K. Neil

Lawrence Livermore National Laboratory, Livermore, California 94550

(Received 1 December 1980)

The design and performance of variable-wiggler, free-electron laser (FEL) amplifiers was studied by using a one-dimensional computer model which incorporated separate sections for design and simulation. Resonant-particle equations were used in the design phase. The variation of the wiggler parameters was not predetermined (linear, exponential, etc.) but was carefully tailored to match the electron energy throughout the FEL amplifier. The simulation section of the model self-consistently tracked the phase-space trajectories of 500 particles for the length of the amplifier. In this way the designs were tested not only for overall gain and efficiency but also for resistance to irregularities in laser input power, electron-beam power, electron-beam-energy spread, and wiggler construction. High-current-density electron beams (electron-beam power > laser-beam power) were found to be essential for stable and efficient amplifiers. Some designs demonstrated better performance under conditions of nonresonant input particles.

I. INTRODUCTION

A free-electron laser (FEL) directly converts the kinetic energy of a high-quality, relativistic electron beam into coherent radiation. It has long been known that this conversion was possible,¹ but it has been shown only recently that relativistic FEL amplifiers could be built.^{2,3} This paper presents the results of a one-dimensional, numerical evaluation of several FEL amplifier designs which incorporate variable-parameter wiggler magnets. Previous numerical investigations of the FEL^{4,5} have studied low-energy, long-wavelength devices which operate principally in the collective-interaction or Raman regime. This work concentrates on higher-energy, shorter-wavelength FEL amplifiers which operate in the single-particle or Compton regime. Our designs are motivated by the possibility that an FEL might be used as an inertial-confinement-fusion driver. We are primarily interested in lasers which exhibit both high single-pass energy extraction and high efficiency. Our designs do not consider quasi-cw recirculating systems which typically extract a small fraction of the electron-beam energy on each pass through the wiggler. FEL amplifiers must also function reliably in the presence of pulse-to-pulse fluctuations in both the electron beam and the laser oscillator. Therefore, we have separated our simulation procedure into two stages. The first stage uses the resonant-particle approximation to design the FEL amplifier. The second stage then tracks individual electrons through the amplifier. This procedure permits us to test FEL performance under non-ideal conditions and to determine which designs are most stable under variations in average beam energy and beam-energy spread.

The design strategy is based on the analysis of the variable-wiggler FEL given by Kroll *et al.*⁶ and reviewed by Szoke *et al.*⁷ This formulation views the FEL amplifier as a coherent-electron decelerator in which the usual longitudinal accelerating field found in LINAC microwave cavities is replaced by a transverse decelerating field provided by the laser. The FEL also requires a spatially transverse, periodic magnetic field in order to provide the requisite coupling between the longitudinally directed electrons and the transverse laser field. In short, in the accelerator the electrons gain energy from the microwave radiation while the converse holds true in the FEL decelerator: The radiation field gains energy from the electrons.

Section II of this paper reviews the major results of the decelerator analysis of the FEL which are used in Sec. III to design FEL amplifiers and in Sec. IV to simulate their operation.

II. BASIC THEORY

A. Single-particle equations of motion

Electron motion in the FEL is governed by Lorentz forces; therefore, each electron's trajectory is specified by

$$m \frac{d\vec{y}}{dt} = -e(\vec{E} + \vec{v} \times \vec{B}). \quad (1)$$

All variables are defined in Table I. The transverse, static, magnetic field is assumed to have the form of a sinusoid with a slowly varying amplitude and period. It is expressed as

$$\vec{B}_w = -B_w(z) \cos\left(\int k_w(z) dz\right) \hat{x}, \quad (2)$$

while the plane-polarized laser fields are written

TABLE I. List of symbols (r subscript refers to the resonant electron).

A_{Δ}	bucket area
B_w	wiggler magnetic field amplitude
b_w	normalized wiggler field, $eB_w/(\sqrt{2}mc)$
c	speed of light
e	electron charge ($e > 0$)
C_{γ}	gain turn-on factor (Eq. 37)
E_s	laser electric field magnitude
e_s	normalized electric field, $eE_s/(\sqrt{2}mc^2)$
E_x	longitudinal space-charge field
e_x	normalized longitudinal space-charge field, eE_x/mc^2
$f(\psi, \gamma)$	electron phase-space distribution function
f_{n0}	Fourier expansion coefficient of $f(\psi, \gamma)$
f_{nr}	Fourier expansion coefficient of $f(\psi, \gamma)$
$F(\psi_r)$	$\cos\psi_r - (\pi/2 - \psi_r) \sin\psi_r$
I	laser intensity
J	electron-beam current density
J_{Δ}	trapped electron-beam current density
$J_{\Delta \text{ min}}$	minimum trapped electron-beam current density required for bucket growth
k_s	laser wave number
k_w	wiggler wave number
L	amplifier length
m	electron rest mass
$P(\psi, \psi_r)$	bucket height
P_{eb}	electron-beam power density
r	electron-beam radius
v	electron velocity
Z_0	impedance of free space
α	phenomenological loss coefficient
γ	electron energy in units of electron rest mass
$\Delta\gamma$	half-width of electron-beam energy distribution
ϵ	electron-beam emittance/ π
ϵ_0	permittivity of free space
φ	phase of laser field
ρ	electron-beam charge density
ω_s	laser frequency
ω_p	plasma frequency $\rightarrow e\rho/m\epsilon_0$
Ω	synchrotron frequency
ψ	relative phase of the electron in the wiggler field to the laser field

$$\vec{E} = E_s(z) \cos\psi_s \hat{y}, \quad (3a)$$

$$\vec{B} = -B_s(z) \cos\psi_s \hat{x}, \quad (3b)$$

where

$$\psi_s = k_s z - \omega_s t + \varphi(z). \quad (3c)$$

A static, longitudinal electric self-field $E_x(z)\hat{z}$ is also included. Our calculations are one dimensional, since these equations do not permit any field variations on the xy plane. (The three-dimensional nature of \vec{B}_w , \vec{E}_s , and \vec{v} can be included in a very approximate manner by defining an equivalent electron energy spread due to transverse effects.) From Eqs. (1), (2), (3a), and (3b), it can be easily shown that the transverse velocity ($v_y\hat{y}$) of the electrons is given by

$$v_y = \frac{e}{m\gamma} \left\{ B_w \sin\left(\int k_w dz\right) / k_w + \frac{E_s \sin\psi_s}{ck_s} \right\}. \quad (4)$$

Equation (4) is derived by assuming that the change in the magnetic field is very small during one magnetic field period. The rate of energy lost by the electron is simply $e\vec{E} \cdot \vec{v}$. This product has components at frequencies ψ_s , $\int k_w dz - \psi_s$, and $\int k_w dz + \psi_s$, but only the last of these varies slowly enough to permit a significant net energy exchange between the electrons and laser field. Therefore, one can write

$$\begin{aligned} \frac{d\gamma mc^2}{dt} &= -e\vec{E} \cdot \vec{v} \\ &= -\frac{e^2 E_s B_w \sin\left(\int k_w dz + \psi_s\right)}{2mk_w \gamma} - ecE_x, \end{aligned} \quad (5)$$

where $v_x = c$ has been assumed in order to derive the final term of Eq. (5). If one now approximates z as equal to ct and uses the normalized field parameters defined in Table I, Eq. (5) may be rewritten as

$$\frac{d\gamma}{dz} = -\frac{e_s b_w}{k_w \gamma} \sin\left(\int k_w dz + \psi_s\right) - e_x. \quad (6)$$

At this point it is convenient to define the phase ψ as

$$\psi = \int (k_w + k_s) dz - \omega_s t + \varphi, \quad (7)$$

so that Eq. (6) becomes

$$\frac{d\gamma}{dz} = -\frac{e_s b_w}{k_w \gamma} \sin\psi - e_x. \quad (8)$$

We will also find it useful to differentiate Eq. (7), which yields

$$\frac{d\psi}{dz} = k_w - \frac{k_s}{2\gamma^2} \left[1 + \left(\frac{b_w}{k_w}\right)^2 - \frac{2e_s b_w}{k_w k_s} \cos\psi + \left(\frac{e_s}{k_s}\right)^2 \right] + \frac{d\varphi}{dz}, \quad (9)$$

where v_y^2 [from Eq. (4)] has been averaged over a wiggler period ($2\pi/k_w$) to determine dz/dt from γ and use has been made of the fact that $\gamma^2/2 \ll 1$. This indicates that if γ , k_w , and b_w are properly chosen, ψ may vary quite slowly. It is also clear that any quantity with frequency $\int k_w dz - \psi_s$ cannot have a spatial frequency less than k_w . This justifies the elimination of these components from Eq. (5).

B. Electromagnetic field equations

Equations (8) and (9) describe the motion of a particular electron in the wiggler field, but the effect of the electron's motion on the laser field has yet to be determined. The longitudinal electric self-field and the amplitude and phase of the laser electric field are determined by the charge and current distributions in the electron beam as specified by the wave equation and Poisson's equation

$$\frac{\partial^2 E_y}{\partial z^2} - \frac{1}{c^2} \frac{\partial^2 E_y}{\partial t^2} = \frac{Z_0 \partial J_y}{c \partial t}, \quad (10a)$$

$$\frac{\partial^2 E_x}{\partial z^2} - \frac{1}{c^2} \frac{\partial^2 E_x}{\partial t^2} = \frac{1}{\epsilon_0} \left(\frac{\partial \rho}{\partial z} + \frac{1}{c^2} \frac{\partial J_x}{\partial t} \right). \quad (10b)$$

We will make the explicit assumption that the charge density is periodic in ψ [Eq. (7)] and take the distribution function of particles in $\psi - \gamma$ space to be $f(\psi, \gamma)$. We are implicitly assuming that the beam may be viewed as a large number of segments of length $2\pi/(k_w + k_s)$ (2π in ψ space) all of which evolve in an identical manner as the electrons move down the amplifier. We normalize f in terms of the charge density, ρ_0 , averaged

over a period in ψ . This average charge density is essentially the uniform density at injection into the FEL, because the particle's axial velocity changes very little during laser amplification. Consequently, we have

$$\rho(\psi) = -e \int f(\psi, \gamma) d\gamma, \quad (11a)$$

and

$$\rho_0 = \frac{-e}{2\pi} \int d\psi \int f(\psi, \gamma) d\gamma. \quad (11b)$$

The current density is written as

$$J(\psi)_{y,z} = -e \int f(\psi, \gamma) v_{y,z}(\gamma) d\gamma. \quad (12)$$

The axial current density averaged over a period in ψ is given by

$$J = \frac{-e}{2\pi} \int d\psi \int f(\psi, \gamma) v_z(\gamma) d\gamma \quad (13a)$$

$$= \rho_0 \langle v_z \rangle, \quad (13b)$$

in which $\langle \rangle$ indicates an average over all particles in a period of ψ . We next substitute Eq. (4) into Eq. (12) to obtain

$$J_y(\psi) = -\left[\frac{e^2 B_w}{m k_w} \sin\left(\int k_w dz\right) + \frac{e^2 E_s}{m c k_s} \sin\psi_s \right] \int f(\psi, \gamma) \frac{d\gamma}{\gamma}. \quad (14)$$

Next expand $f(\psi, \gamma)$ in a Fourier series as shown below:

$$\int \frac{f}{\gamma} d\gamma = f_0 + \sum (f_{ne} \cos n\psi + f_{no} \sin n\psi), \quad (15a)$$

with

$$f_{ne} = \frac{1}{\pi} \int \frac{f}{\gamma} \cos n\psi d\gamma d\psi, \quad (15b)$$

and

$$f_{no} = \frac{1}{\pi} \int \frac{f}{\gamma} \sin n\psi d\gamma d\psi. \quad (15c)$$

When Eq. (15a) is substituted into Eq. (14) it is apparent that the only portion of J_y that is synchronous with the laser field is the $n=1$ term in the series. The synchronous portion of the current density J_s is given by

$$J_s = \frac{e^2 B_w}{2m k_w} (f_{1e} \sin\psi_s - f_{1o} \cos\psi_s) - \frac{e^2 E_s}{m k_s c} f_0 \sin\psi_s. \quad (16)$$

If the amplitude and phase of E_y vary slowly with z , we may employ the slowly varying envelope approximation (SVEA)⁸ and rewrite Eq. (10a) as

$$-2k_s \left(\frac{d\varphi}{dz} E_s \cos\psi_s + \frac{dE_s}{dz} \sin\psi_s \right) = \frac{Z_0 \partial J_y}{c \partial t}. \quad (17)$$

We combine this relation with Eq. (16) and equate the sine and cosine terms to obtain

$$\frac{dE_s}{dz} = \frac{eb_w}{\sqrt{2}2k_w} Z_0 c f_{i0}, \quad (18a)$$

$$\frac{d\varphi_s}{dz} = \frac{eZ_0c}{2\sqrt{2}E_s} \left(\frac{b_w f_{1s}}{k_w} - \frac{2e_s f_0}{k_s} \right). \quad (18b)$$

We make the approximation $v_x = c$ in Eq. (13) so that Eq. (18) may be rewritten as

$$\frac{dE_s}{dz} = \frac{Z_0 b_w}{\sqrt{2}k_w} |J| \left\langle \frac{\sin\psi}{\gamma} \right\rangle - \alpha E_s, \quad (19a)$$

$$\frac{d\varphi_s}{dz} = \frac{Z_0 b_w}{\sqrt{2}k_w} \frac{|J|}{E_s} \left\langle \frac{\cos\psi}{\gamma} \right\rangle - \frac{k_s \omega_p^2}{2\gamma \omega_s^2}. \quad (19b)$$

We have used Eqs. (15b) and (15c) to define

$$\left\langle \frac{\sin\psi}{\gamma} \right\rangle = \frac{\int [f(\psi, \gamma)/\gamma] \sin\psi \, d\psi \, d\gamma}{\int f(\psi, \gamma) \, d\psi \, d\gamma}, \quad (20a)$$

and

$$\left\langle \frac{\cos\psi}{\gamma} \right\rangle = \frac{\int [f(\psi, \gamma)/\gamma] \cos\psi \, d\psi \, d\gamma}{\int f(\psi, \gamma) \, d\psi \, d\gamma}. \quad (20b)$$

The longitudinal electric self-field E_x obeys Eq. (10b), which may be replaced by the simple relation

$$\frac{dE_x}{d\psi} = \frac{[\rho(\psi) - \rho_0]}{(k_w + k_s)\epsilon_0}. \quad (21)$$

This equation is numerically solved using Eq. (11a), a finite-difference method and periodic boundary conditions.

The wiggler designs to be described in Sec. III do not include E_x , but the simulations described in Sec. IV do include E_x in the equations of motion. Terms oscillating at the frequency $\int k_w dz - \psi_s$ are once again assumed to average out to zero very quickly. Equations (8), (9), (19a), and (19b) now describe the one-dimensional motion of any electron in the specified fields. The self-consistency of these equations may be demonstrated by using Eq. (19a) and conservation of energy to recover Eq. (8).

C. Resonant-particle approximation

We are primarily concerned with the solution of Eqs. (19a), (19b), and (21) for the growth of the laser field. Unfortunately, in order to determine $f(\psi, \gamma)$, the simultaneous solution of $2n+3$ differential equations (where n is the number of electrons in the electron beam) is required. How-

ever, the details of the individual electron motion are of secondary importance. Therefore, we attempt to solve Eqs. (8) and (9) for one average electron, thus permitting the multivariable functions $\langle \sin\psi/\gamma \rangle$ and $\langle \cos\psi/\gamma \rangle$ in Eqs. (19a) and (19b) to be replaced by functions of only two variables—the energy and phase of an “average electron.” Other authors^{6,7} have shown that this is a good approximation for those electrons with energy γ and phase ψ which satisfy the following condition:

$$\begin{aligned} |\gamma - \gamma_r| &\leq P(\psi, \psi_r) \\ &= \left(\frac{e_s b_w}{k_w^2} \right)^{1/2} [\cos\psi + \cos\psi_r - (\pi - \psi - \psi_r) \sin\psi_r]^{1/2}, \end{aligned} \quad (22)$$

where γ_r and ψ_r are the energy and phase of the average electron. Equation (22) was derived by choosing an average electron with the specific property that its energy varies in precisely the manner required to keep its phase nearly constant. That is,

$$\frac{d\psi_r}{dz} \ll \Omega_{s\gamma r}, \quad (23a)$$

where

$$\Omega_{s\gamma r} = (2b_w e_s \cos\psi_r / \gamma_r^2)^{1/2}. \quad (23b)$$

An electron with this property is usually called a resonant electron. Other electrons which satisfy Eq. (22) will, on the average, track the motion of the resonant electron. Equation (22) was obtained by linearizing the energy deviation between the resonant and nonresonant electrons and looking for conditions under which the nonresonant electron's motion is trapped about the resonant motion. This approximation is only accurate when $|\gamma_r - \gamma|/\gamma$ is small. Space-charge fields are usually small,⁹ therefore e_x in Eq. (8) was ignored in deriving Eq. (22). Equation (22) defines a region in phase space (γ, ψ) in which electron orbits are closed and stable. This region is called a bucket by accelerator designers,¹⁰ and we designate with the label Λ quantities associated with particles inside the bucket. We define A_Λ to be the area of the phase-space region delimited by Eq. (22),

$$A_\Lambda(\psi_r) = 2 \int P(\psi, \psi_r) \, d\psi. \quad (24)$$

This procedure permits us to simplify the system of Eqs. (8), (9), (19a), and (19b) to the following set of equations:

$$\frac{d\gamma_r}{dz} = -\frac{e_s b_w}{k_w \gamma_r} \sin\psi_r, \quad (25)$$

$$\frac{d\psi_r}{dz} = k_w - \frac{k_s}{2\gamma_r^2} \left[1 + \left(\frac{b_w}{k_w} \right)^2 - \frac{2e_s b_w}{k_w k_s} \cos\psi_r + \left(\frac{e_s}{k_s} \right)^2 \right] + \frac{d\varphi}{dz}, \quad (26)$$

$$\frac{dE_s}{dz} = \frac{Z_0 b_w J_\Lambda}{\sqrt{2k_w} \gamma_r} \langle \sin\psi \rangle_\Lambda - \alpha E_s, \quad (27a)$$

$$\frac{d\varphi}{dz} = \frac{Z_0 b_w J_\Lambda}{\sqrt{2k_w} E_s} \langle \cos\psi \rangle_\Lambda \quad (27b)$$

(where J_Λ is the current density within the bucket),

$$\langle \sin\psi \rangle_\Lambda = \frac{2}{A_\Lambda} \int P(\psi, \psi_r) \sin\psi \, d\psi, \quad (28a)$$

and

$$\langle \cos\psi \rangle_\Lambda = \frac{2}{A_\Lambda} \int P(\psi, \psi_r) \cos\psi \, d\psi. \quad (28b)$$

We ignore the electrostatic term (e_s) when deriving the resonant-particle equations because our simulations (which do include e_s) have shown that the longitudinal field has only a very small effect on the amplifier's performance. In writing Eqs. (28a) and (28b), we have assumed that the electrons fill the bucket with uniform phase-space density and have ignored the variation of γ within the bucket. Both $\langle \cos\psi \rangle_\Lambda$ and $\langle \sin\psi \rangle_\Lambda$ are now functions of a single variable ψ_r , and may be readily computed. It should be remembered that when one assumes that a nonresonant electron exhibits behavior similar to the resonant electron, one is ignoring the synchrotron motion of the nonresonant electron.

Of course, all of the electrons in the electron beam may not fall in the bucket. The question then arises as to how to treat the untrapped electrons. In the resonant-particle approximation, the untrapped electrons do not contribute to the laser-field growth and can be ignored. Thus the laser gain is only proportional to the number of electrons within the bucket. Equations (25)–(28) do not need any further corrections.

Equations (25), (26), (27), and (28) serve as the basis for the FEL designs. The design procedure is described in Sec. III. A simulation is later used to test the accuracy of the approximations made in order to obtain the design equations, particularly the concept of buckets. Therefore, the simulation will use Eqs. (8) and (9) for each electron and simultaneously solve $2n+3$ differential equations.

III. FEL DESIGN

A successfully designed FEL amplifier must continuously decelerate a large fraction of the electron beam. We base our designs on the assumption that this can be accomplished if the resonant particle is decelerated and simultaneously the bucket area is kept large. This strategy is supported by Liouville's theorem which states that phase-space density remains constant in an

adiabatic process. As long as the deceleration is nearly adiabatic, one may expect large trapping fractions. Therefore, the design problem reduces to finding a solution to Eqs. (25)–(28) for $\lambda_w(z)$ and $B_w(z)$, which simultaneously satisfies our two design goals—restricting ψ_r to be between 0 and $\pi/2$, and maintaining A_Λ large.

The resonant-particle motion is specified by four equations [Eqs. (25), (26), (27a), and (27b)], and the bucket area is specified by one additional equation (24). There are seven unknowns (γ_r , ψ_r , E_s , φ_s , A_Λ , b_w , and λ_w) in these five equations; consequently, in order to specify a design one must have two additional constraints. These constraints are completely arbitrary and must be chosen by the FEL designer. In addition, a consistent set of initial conditions must be chosen. We have considered only a few of the many possible options. A sixth equation is selected from the following list:

$$\frac{d\lambda_w}{dz} = 0 \quad (29a)$$

(constant wiggler period);

$$\frac{db_w}{dz} = 0 \quad (29b)$$

(constant magnetic field amplitude); and

$$\frac{d(b_w/k_w)}{dz} = 0 \quad (29c)$$

(constant magnetic vector potential); while a seventh equation is chosen to be either

$$\frac{d\psi_r}{dz} = 0 \quad (30a)$$

(stable phase deceleration), or

$$\frac{dA_\Lambda}{dz} = \text{const} \quad (30b)$$

(programed bucket area deceleration).

Option (30b) is practical only when high-current-density electron beams are used.¹¹

The initial values of γ_r , λ_w , λ_s , ψ_r are iteratively selected to illustrate FEL scaling and high-power FEL amplifier performance. The initial magnetic field is chosen so that $d\psi_r/dz = 0$ at $z = 0$ [Eq. (26)]. The initial laser field is chosen to make the maximum bucket height equal to half the maximum energy spread in the electron beam, that is,

$$e_s(z=0) = \frac{(k_w \Delta\gamma)^2}{2b_w F(\psi_r)}, \quad (31a)$$

where

$$\Delta\gamma = (\gamma_{\text{max}} - \gamma_{\text{min}})/2. \quad (31b)$$

This condition implies that all our designs assume that amplifiers will operate with full buckets. This minimizes the input laser flux required for a given electron decelerator. $A_\Lambda(z=0)$ is now calculated from Eq. (24) and $\varphi(z=0)$ is set to 0. We then estimate the required trapped current by writing

$$J(z)_\Lambda = J \frac{A_\Lambda(z)}{2\pi(2\Delta\gamma)}. \quad (32)$$

We impose the additional restriction that $J_\Lambda(z) \leq J_\Lambda(0)$, for all z . Actually, this is a conservative estimate of the bunched current density.

Clearly if one chooses option (30a) (stable phase deceleration) and an initial ψ_r between 0 and $\pi/2$, the first design goal is satisfied. The second goal is met if

$$\frac{dA_\Lambda}{dz} \geq 0. \quad (33)$$

If one assumes that $d\psi_r/dz = 0$, Eq. (33) reduces to

$$\frac{b_w}{k_w^2} \frac{de_s}{dz} + e_s \frac{d}{dz} \left(\frac{b_w}{k_w^2} \right) \geq 0. \quad (34)$$

The second term is negative for all of our designs,¹² and therefore the bucket can only be kept large if the laser field grows strongly. This can only be accomplished if the current density is sufficiently high. Now by utilizing Eqs. (26), (29a), (30a), and (31), and neglecting terms of order e_s/k_s , one finds that satisfying Eq. (34) (at $z=0$) requires that

$$J_{\Lambda \text{ min}} \geq \frac{\gamma_r k_w^2 (\Delta\gamma)^2}{k_w b_w^4 F^2(\psi_r)} \frac{mc^2}{eZ_0}. \quad (35)$$

This condition may also be expressed as the ratio between the electron-beam power and the laser-beam power by writing

$$\frac{P_{\text{eb}}}{I} \geq 2 \left(\frac{k_w^2}{b_w^2} + 1 \right). \quad (36)$$

Although Eqs. (35) and (36) were derived for a constant wiggler period, stable phase deceleration amplifier, similar expressions may be derived for all of the design options.¹¹ Note that both the input laser intensity [Eq. (31)] and the required minimum current density depend on the fourth power of the electron-beam energy spread. This places a premium on quality electron beams. If one wishes to maintain a growing bucket not only at $z=0$, but throughout the decelerator, one must supply a trapped current density much greater than the minimum current density specified in Eq. (35). Therefore one does not expect these designs to perform well unless J_Λ is much greater than $J_{\Lambda \text{ min}}$. For example, one must have J_Λ

$\geq 7J_{\Lambda \text{ min}}$ when design option (29a) (constant wiggler period) is picked to ensure that A_Λ is larger at the end of the amplifier (25% deceleration) than it was at the beginning of the amplifier.

It follows from Eqs. (35) and (36) that eventually the bucket must shrink, because the laser energy is increasing at the expense of the electron-beam energy. In order to prevent the loss of electrons from a full bucket, the laser-beam energy cannot become larger than $\frac{1}{2}$ of the trapped electron-beam energy [for option (29a), constant wiggler period]. This figure becomes $\frac{3}{8}$ for a design which maintains a constant equivalent energy spread from transverse motion [cf. Eq. (38), below]. Although a slight improvement on these figures is possible by designing with option (30b) (programed bucket area deceleration), there is clearly a maximum amount of energy which can be extracted from the electron beam in a controlled (no detrapping) manner. This limits the efficiency of the FEL amplifier. If one is willing to allow significant numbers of electrons to become detrapped, more energy can be extracted. This remains true even when design option (30b) (programed bucket area deceleration) is chosen for designs.

Unfortunately, these design equations assume that the electron beam is already bunched, while a realistic FEL amplifier must utilize an unbunched beam. This discrepancy has a detrimental effect on FEL performance. We have allowed for an initially unbunched beam by replacing $\langle \sin\psi \rangle_\Lambda$ and $\langle \cos\psi \rangle_\Lambda$ in Eqs. (27a) and (27b) with $C\langle \sin\psi \rangle_\Lambda$ and $C\langle \cos\psi \rangle_\Lambda$, where we arbitrarily choose

$$C = 1 - \exp\{[\gamma_r(z) - \gamma_r(0)]C_r / \Delta\gamma\}. \quad (37)$$

This allows the bunch to form slowly and partially compensates for the initial absorption of laser power by electrons not found within the bucket. After the resonant particle has been decelerated by more than a few times the initial energy spread of the beam, the resonant-particle description should be more accurate and wiggler design may proceed accordingly. The addition of the factor "C" to Eq. (27) is only a design strategy used to model bunch formation. This factor is not included in the simulation described in Sec. IV.

The design problem is now completely specified, and one merely has to numerically integrate Eqs. (25), (26), (27), (28) [(29a), (29b) or (29c)], and (30a) or (30b) in order to calculate $\lambda_w(z)$ and $b_w(z)$ and estimate the FEL amplifier performance [$e_s(z)$]. Note that this procedure results in a wiggler carefully matched to the electron energy throughout the FEL amplifier and should be distinguished from designs which arbitrarily select

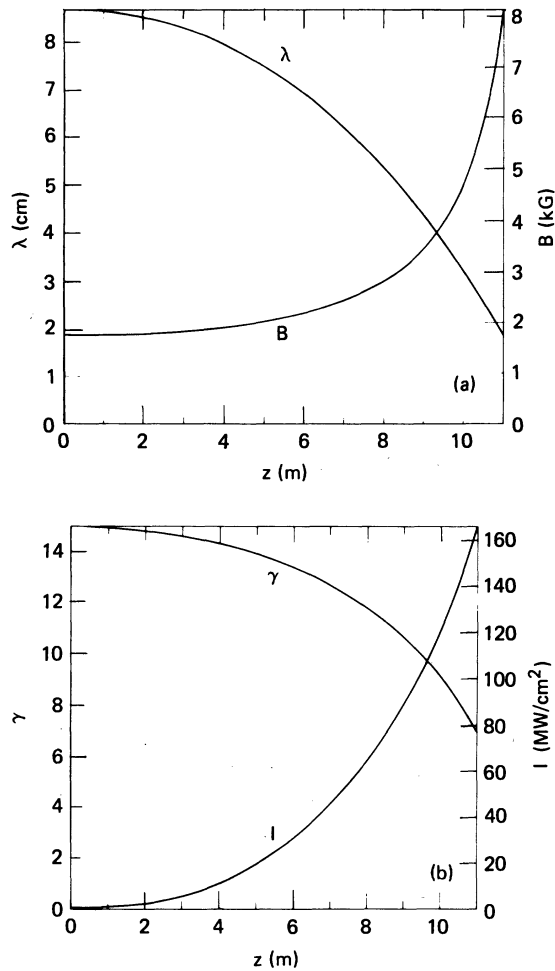


FIG. 1. Design and estimated performance of a 385- μm FEL amplifier of constant magnetic potential (b_w/k_w) and stable phase angle.

a wiggler taper (e.g., exponential or linear).

We have used the procedure described above to design a high-power, 385- μm FEL amplifier. We chose $\gamma_r = 15$, $\psi_r = 0.4$, $\Delta\gamma = 0.2$, $\lambda_w = 8.7$ cm, $C_r = 1.0$, and $J = 100$ A/cm². The estimated trapped current density is then 41 A/cm², well above the minimum required trapped current density of 0.35 A/cm². An input laser flux of 0.67 MW/cm² is also required.¹³

The design resulting from these initial conditions and options (29c) and (30a) (constant magnetic vector potential and stable phase deceleration) is illustrated in Fig. 1. In 11 meters the magnetic field has increased from 1.7 to 8 kG, while the wiggler spacing has decreased from the initial 8.7 to 2 cm. The laser field is predicted to reach over 160 MW/cm² at this point, while γ has decreased to 7 (no losses were included in this

design). These calculations also indicate that the bucket area has increased by a factor of 2 in 11 meters, and therefore our design goals have been met. Our one-dimensional arguments lead us to expect this device to perform well. Unfortunately, a sinusoidal wiggler field requires that there also be a transverse variation of the magnetic field. The transverse field has an effect similar to that of introducing an additional equivalent energy spread of magnitude¹⁴

$$\Delta\gamma_{\text{eff}} = \gamma_r \frac{b_w^2 \gamma^2}{4(1 + b_w^2/k_w^2)} \quad (38)$$

into the beam. Upon examining the design for the constant b_w/k_w wiggler we find that the equivalent energy spread (assuming constant r) has increased 10 times while the bucket area has increased 80%. Equation (38) can be reexpressed in terms of the electron-beam emittance as¹⁵

$$\Delta\gamma_{\text{eff}} = \gamma_r \frac{(\gamma\epsilon) b_w}{4(1 + b_w^2/k_w^2)}. \quad (39)$$

If we assume that the electron-beam normalized emittance ($\gamma\epsilon$) stays constant (the beam radius shrinks) we find that the equivalent energy spread still increases more than the bucket area. Severe detraping would result. Therefore, although our one-dimensional model would predict good performance for this design, two-dimensional arguments lead us to disregard option (29c) (constant magnetic vector potential).

The magnetic field profile and expected laser gain in a constant-period 385- μm FEL amplifier are illustrated in Fig. 2. The magnetic field decreases from 1.7 to 0.17 kG in 13 meters while the laser field grows to 88 MW/cm² and the average electron energy decreases to $\gamma = 10.9$. As Fig. 2c shows, the bucket area is equal to or greater than the initial bucket area for 95% of the amplifier while the additional energy spread due to transverse-field variations [Eqs. (38) and (39)] has actually decreased. Therefore, this design is expected to perform well. Unfortunately, this design only permits one to decelerate the electrons by 30%. This problem may be rectified without increasing the effective energy spread by either increasing the initial electron energy, or by allowing λ_w to decrease [with a constant b_w section, option (29b)] only after b_w has been reduced below its initial value. The FEL design resulting from a variation of this second alternative is illustrated in Fig. 3(a). We choose options (29a) and (30b) (constant wiggler period, programmed bucket area deceleration), and options (29b) and (30b) (constant magnetic field, programmed bucket area deceleration), both with

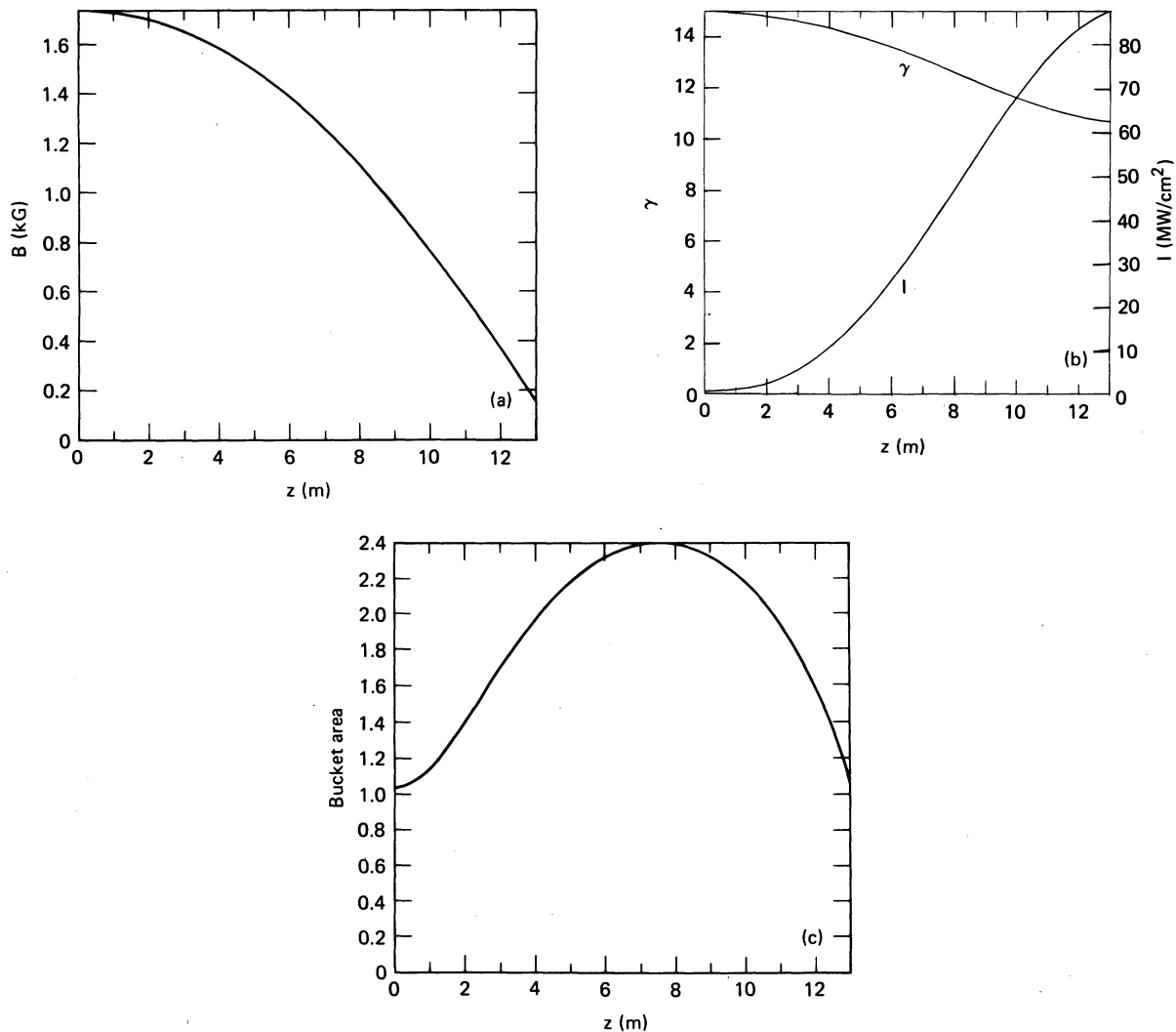


FIG. 2. Design and estimated performance of a 385- μm FEL amplifier with a constant period and a stable phase angle.

$dA/dz = 0$. During the first 5.5 meters, λ_w is held constant and b_w decreases from 1.7 to 1.1 kG. For the next 5.5 meters, λ_w decreases while b_w is held constant. As illustrated in Fig. 3(b), ψ_r is programmed to change in the precise manner required to keep the bucket area constant. Figure 3(c) illustrates this laser's output power as a function of amplifier length. Almost $150 \text{ MW}/\text{cm}^2$ may be obtained in 11 meters, almost as much as in the constant b_w/k_w design but without the added problems of detrapping due to excessive transverse-field fluctuations. An alternative design to option (29) which would eliminate the problem of detrapping due to inhomogeneous transverse-magnetic fields might be obtained by requiring $\Delta\gamma$ equivalent to remain constant throughout the

accelerator. The detrimental effects of electron-beam emittance are similar to those of transverse-magnetic field fluctuations, and therefore designs which avoid the latter problem also prevent the former.

The particular design parameters used in these examples were chosen for two reasons:

(1) They illustrate the important phenomena one would expect to observe in a high-power, high-gain FEL amplifier.

(2) They describe a device which can be built with current technology. Simple scaling considerations allow one to extend these designs to different laser wavelengths and electron-beam energies. For example, if $J/J_{\text{A min}}$ and b_w/k_w

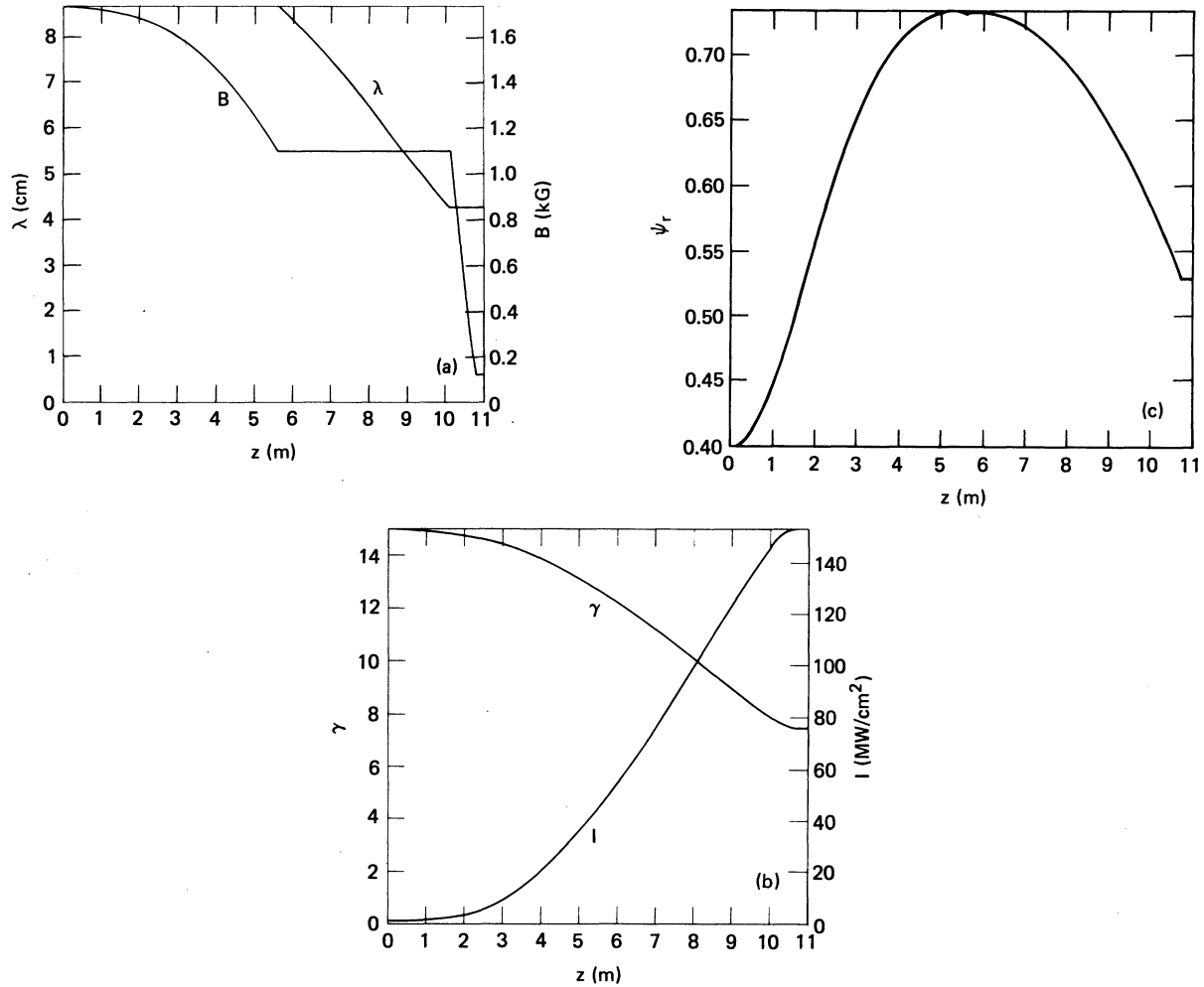


FIG. 3. Design and estimated performance of a 385- μm FEL amplifier with a combination design—constant wiggler period, programmed bucket area and constant magnetic field, programmed bucket area.

are held constant, the amplifier length for fixed $I_{\text{out}}/I_{\text{in}}$ scales as

$$L \propto \left(\frac{\gamma_r}{\Delta\gamma} \right)^2 \lambda_w. \quad (40)$$

One may demonstrate this design scaling with a 250-nm FEL amplifier design comparable to that shown in Fig. 3 for a doubled wiggler period (17.4 cm), and a fourfold reduction in energy spread ($\Delta\gamma/\gamma = 0.33\%$, C_r reduced by a factor of 4 to preserve design scaling). Although J_A is now 7.27 kA/cm², J/J_{min} remains unchanged. As predicted by Eq. (39), the only difference between Figs. 4 and 3 is a 32-fold increase in length.

These four examples illustrate how one can rapidly design a tapered-wiggler FEL. One must, of course, determine if these designs perform as expected when the resonant-particle approxima-

tions leading to Eqs. (25)–(28) and the concept of buckets are relaxed. This task is performed by the simulation discussed in Sec. IV.

IV. FEL SIMULATION

The purpose of the FEL simulation described in this section is fourfold.

- (1) To investigate the validity of the bucket approximation to the gain equation (27a).
- (2) To study the initial bunching of the electrons and to evaluate the trapping efficiency of several different wiggler designs.
- (3) To determine the lifetimes of the buckets or, in other words, to determine if the electrons can be kept in the bucket for a period long enough to achieve substantial amplification.
- (4) To determine the stability of the FEL amp-

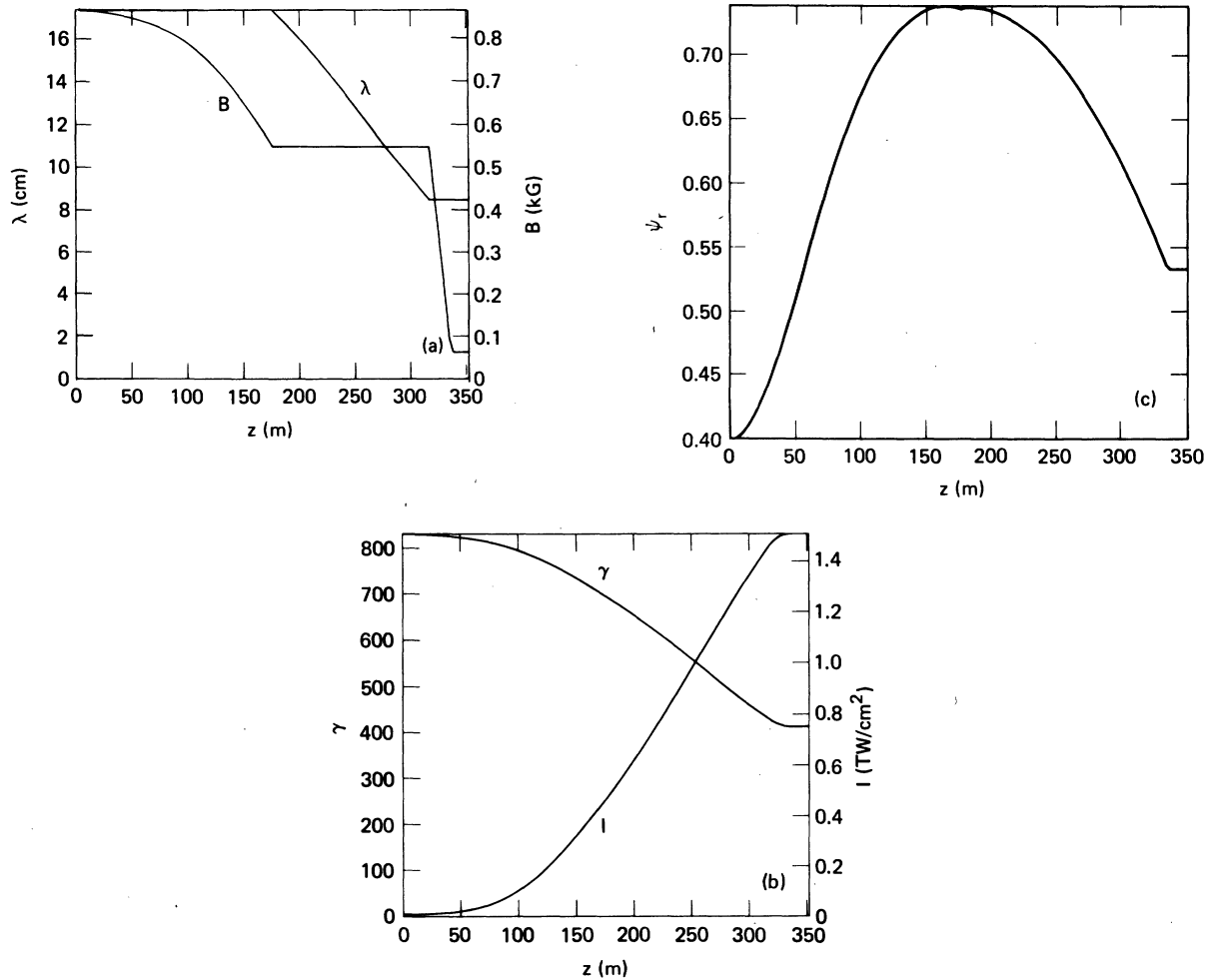


FIG. 4. Design and estimated performance of a 250-nm FEL amplifier with a combination design—constant wiggler period, programmed bucket area, and a constant magnetic field, programmed bucket area. Scaled version of the design which is illustrated in Fig. 3.

lifier designs against input fluctuations in electron-beam voltage, current, energy spread, laser oscillator power, and wiggler irregularities.

The simulation has several limitations. Most important, it is one dimensional. It does not account for any transverse inhomogeneities in either the wiggler field or the laser field.¹⁵ For example, by using Eqs. (27a) and (27b), we can estimate the total optical phase change in an FEL amplifier as

$$\varphi(z) - \varphi(0) \approx \frac{1}{2 \tan \psi_r} \ln \frac{I(z)}{I(0)}. \quad (41)$$

A high-gain amplifier yields a large $\Delta\varphi$ which might lead to self-focusing of the laser beam and subsequent detrapping. This effect, along with possible diffraction compensation, has been ig-

nored. We have only considered a monochromatic laser field; the disadvantages (and possible advantages) of a multicolor laser field have been ignored in the present work. Finally, we will not discuss the synchrotron instability discussed by Kroll.¹⁶ As we stated previously, we have included the effects of the longitudinal electric self-field that results from the electron bunching.

Operation of the FEL amplifier is simulated by numerical integration of Eqs. (8) and (9) and calculation of the one-dimensional phase trajectories (γ, ψ) of 500 electrons as they traverse the previously designed wigglers. Field growth is simultaneously determined from Eqs. (19a) and (19b).

Figure 5 illustrates the results of this process for the wiggler design illustrated in Fig. 2. Figure 5(a) shows the initial position of the electrons in phase space. Random loading of the electrons

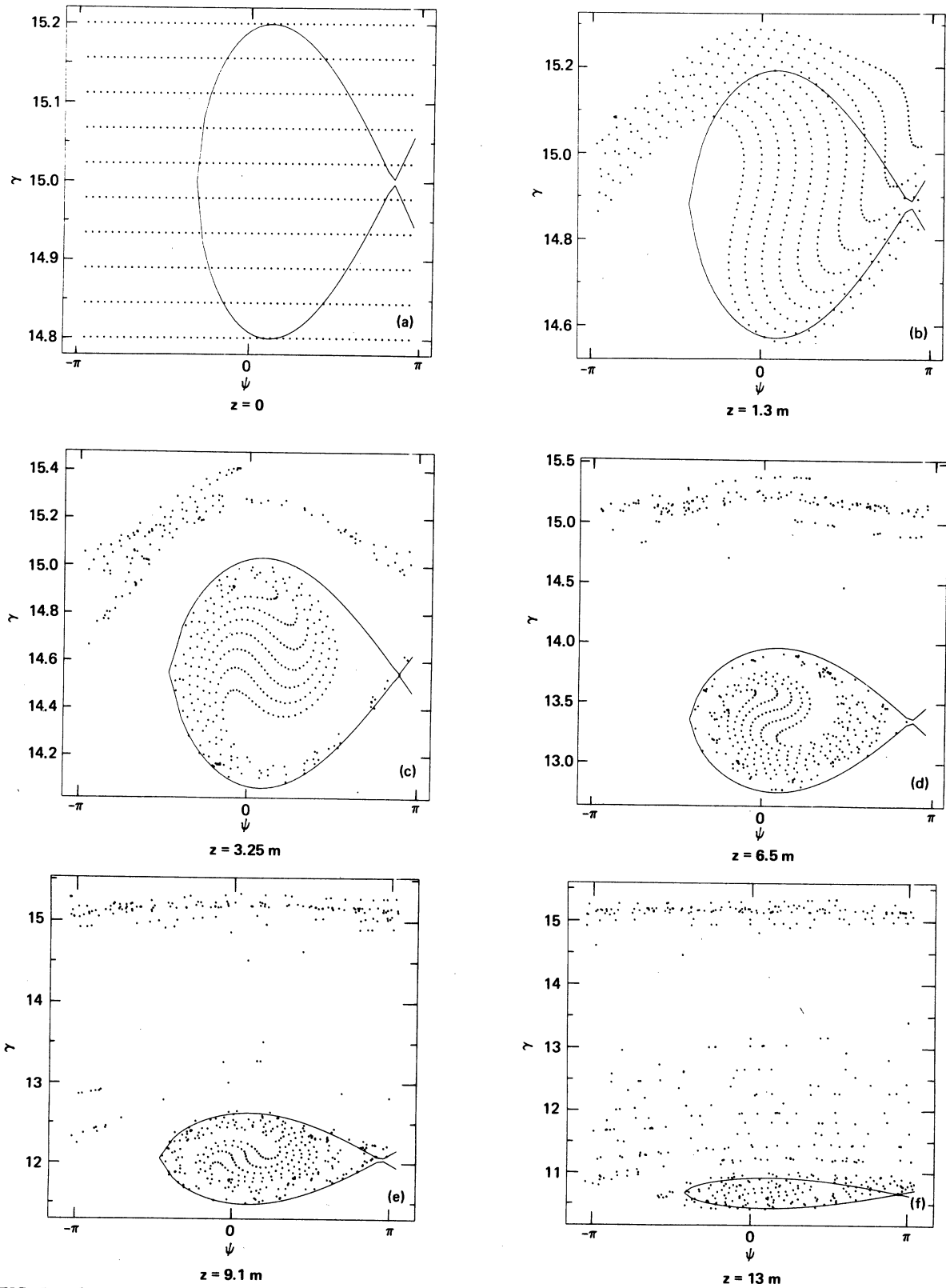


FIG. 5. Electron phase-space evolution in a 385- μm FEL amplifier obtained from the simulation of the FEL design shown in Fig. 2 at $z = 0, 1.3, 6.5, 9.1,$ and 13 meters. [Note that the vertical scale increases in (a)–(f).]

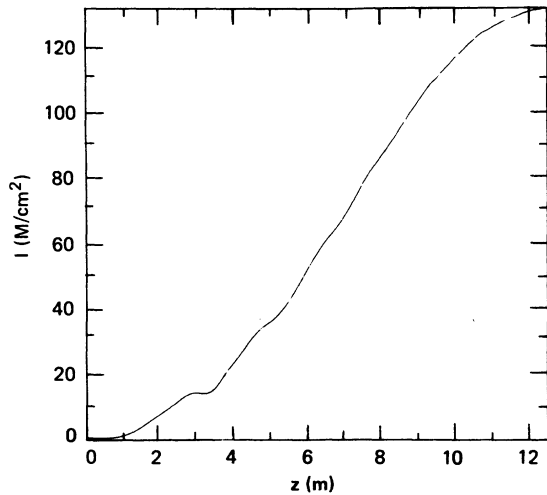


FIG. 6. Laser intensity of a 385- μm FEL amplifier of constant period and stable phase angle predicted by a one-dimensional simulation of the FEL design shown in Fig. 2.

would have been more precise, but as our results are only meant to demonstrate qualitative FEL behavior, we have chosen the pattern illustrated. The phase-space area which we have called a bucket is denoted by the solid fish-shaped curve. Figure 5(b) shows the phase-space position of each electron after it has traversed the first 1.3 meters of the wiggler. The electrons are beginning to bunch in the bucket. Figures 5(c), 5(d), and 5(e) illustrate that after 3.25, 6.5, and 9.1 meters, respectively, the electrons do in fact separate into two distinct groups, one of which is not decelerated, the other of which fills the bucket and decelerates. Figure 5(f) illustrates the phase-space position of the electrons after they have traversed 13 meters of the wiggler. Note that detrapping began at about $\gamma_r = 13$ and became appreciably worse as the electrons continued to decelerate.

Figure 6 illustrates the growth of the laser field which results from the energy lost by the decelerated electrons. If one compares Figs. 6 and 2, one sees that the simulation predicts a laser gain of 1.5 times larger than that predicted by the design equations. This can only occur if more electrons are trapped than was estimated by Eq. (32).

The reason for the excess trapping may be determined by examining which electrons become trapped as a function of design current density. Figures 7(a)–7(c) replot the initial phase-space distribution, but those electrons which are still located within the bucket after γ_r has been reduced by 25% are designated in boldface. At low current densities [Fig. 7(a), $J_A/J_{A,\text{min}} = 0.12$], the number and location of the electrons which are trapped is

much less than that predicted by Eq. (26) because the low current density is incapable of supporting a field growth sufficient to maintain bucket growth. However, as the current density increases, the fraction of electrons trapped increases. One finds that when $J_A/J_{A,\text{min}} \approx 7$ [Fig. 7(b)], the number of electrons trapped is slightly less than that predicted by Eqs. (24) and (32) because the initial bunching did not effectively capture all the electrons located within the bucket. The overestimate of electrons captured during the design stage also leads to an overestimate of the laser field. Therefore, during the simulation, the bucket must readjust by increasing its phase angle to one slightly above the design angle [approximately 0.5 in Fig. 7(b)]. This also leads to a loss of electrons. As is shown in Fig. 7(c), trapping continues to increase as the current density increases. Furthermore, trapping is stronger for electrons below the design energy than above. The increased trapping results from the fact that a strongly growing laser field enlarges the bucket. The preference for lower-energy electrons occurs because the bucket is decelerating, a circumstance which allows the low-energy electrons to catch up. The process is aided by the slight modifications to the resonant-particle equations introduced into the design equations with the parameter C_r . In fact, for large design C_r ($C_r > 1$) the excess trapping is reduced. A decreased design C_r enhances trapping. The net result is that high current densities promote high trapping efficiencies. This explains why the laser-field growth is larger in our simulation than our designs predicted. As will be shown subsequently, FEL stability is also enhanced.

The initiation of detrapping at $\gamma = 13$ in the example illustrated by Fig. 6 may be simply explained. According to Fig. 2(c), the bucket area reaches a maximum at about 7.5 meters or where $\gamma_r = 12.9$. This is the point at which the condition expressed by Eq. (36) is no longer satisfied. The bucket must shrink. Although the bucket is larger than it was initially, once it begins to shrink the excess electrons which were trapped because of the enlargement of the bucket are lost. Finally, after 13 meters the bucket is back to its original size [note the varying vertical scale in Figs. 5(a)–5(f)], and one is left with just those electrons found in the bucket at $z = 0$.

One can prevent the bucket from shrinking by switching to a growing bucket design option (30b) at $\gamma_r = 13$. Simulations indicate that when this is done, detrapping is greatly reduced. The penalty for this choice is an increase in amplifier length.

A further examination of Fig. 7(c) leads one to suspect that an initial average electron energy below the design energy will promote better trapping.

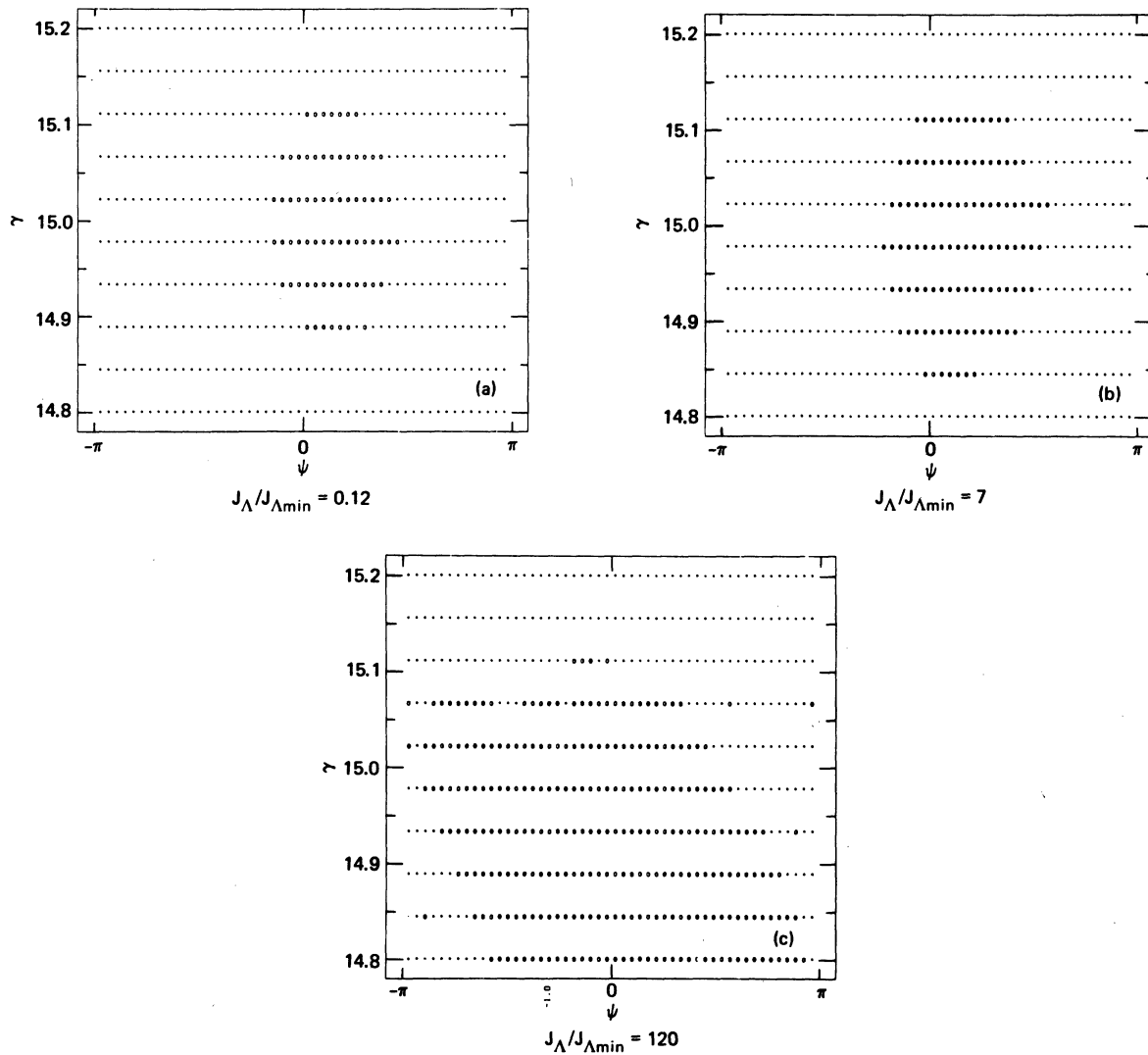


FIG. 7. Phase-space distribution of electrons still trapped (indicated by boldface type) after they have been decelerated by 25% in a 385- μm FEL amplifier for current density ratios $J_A/J_{\Lambda\min} = 0.12, 7,$ and 120 .

This possibility was investigated by plotting the fraction of electrons trapped in our 385- μm FEL after 25% deceleration of the resonant electron as a function of design current for initial electron energy 1.3% above and 1.3% below the design energy $\pm\Delta\gamma$, and at the resonant energy. The results are illustrated in Fig. 8. At low current densities the fraction of electrons still trapped at $\gamma_r = 11.25$ is approximately 15%, appreciably less than the 41% estimated by Eq. (32). When the energy is displaced by one-half the bucket height, the fraction of trapped electrons is reduced by almost 50% (one-half the bucket height), as one would expect. As the current density increases, the fraction trapped increases for both the resonant case and

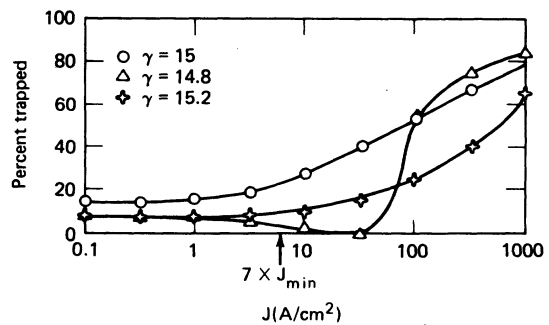


FIG. 8. Percent of electrons still trapped after 25% deceleration in a 385- μm FEL amplifier as a function of both initial conditions and design current density.

the high-energy case. Fortunately, as the current density increases further, trapping continues to increase because of the growth of the bucket.

The behavior of the amplifier when the initial electron energy is below design specifications is considerably more complicated. Low-energy electrons initially absorb energy from the radiation field, which causes the bucket area to shrink. The higher the current density, the stronger the absorption and the more the bucket shrinks, further reducing trapping. However, as Fig. 8 shows, at yet higher current densities this trend is reversed, because the field drops so sharply that low-energy electrons momentarily stop decelerating and come into synchronism with the wiggler field. Low-energy electrons tend to fill the low- γ portion of the bucket (the bottom half of the potential well), which results in better trapping than was observed for the resonant electrons. This is a consequence of the decelerating bucket. It should be pointed out that at extremely high current densities, although space charge is not a problem, the gain is so high that the approximations leading to Eqs. (8) and (9) become suspect.

Our simulations have also shown that low-energy electrons can be trapped at low current densities if we use FEL designs formulated with reduced C_r . This reduction is similar to the drop in electric field discussed above, i.e., it reduces the laser gain and electron deceleration, allowing the bucket and the electrons to achieve synchronism at some distance down the wiggler. In general, de-

creasing C_r in our designs increases the stability of the amplifier (i.e., both resonant and high-energy electrons are trapped well, and low-energy electrons are trapped very well). The disadvantage to reducing C_r is that the laser gain is also reduced.

We have attempted to examine the performance of our 385- μm FEL designs when the operating parameters are altered slightly from those specified in the design. Accordingly, we have run our simulation for the type of design shown in Fig. 2 (i.e., $d\psi_r/dz = 0$, $d\lambda_w/dz = 0$) under the following conditions:

- | | |
|--|--------------------------------|
| (1) $\gamma_0 = 1.013\tilde{\gamma}_0$, | (6) $I_0 = 2\tilde{I}_0$, |
| (2) $\gamma_0 = 0.987\tilde{\gamma}_0$, | (7) $B = \pm 0.015\tilde{B}$, |
| (3) $\Delta\gamma = 0.75$, | (8) $B = \pm 0.025\tilde{B}$, |
| (4) $\Delta\gamma = 1.25$, | (9) $J = 0.32\tilde{J}$, |
| (5) $I_0 = 0.5\tilde{I}_0$, | (10) $J = 3.2\tilde{J}$. |

Injection values are indicated by a subscript zero, and design values are indicated by a tilde. All initial conditions except the current density \tilde{J} are the same as for the design in Fig. 2. Conditions (7) and (8) were simulated by changing the smooth magnetic field profiles specified by the design algorithm into a series of constant magnetic field steps which remain within the limits specified above.

The results for several different design current densities are given in Table II by listing the percentage of electrons still trapped after γ_r has been decelerated to 75% of its initial value. Also listed

TABLE II. Performance of nine FEL designs as operating parameters are varied. Each column is a particular FEL design. The first two rows give the design current and length required to reduce γ_r from 15 to 11.25. The remaining rows give results of particle simulation, when one input parameter for each row is altered and show the percentage of input particles still trapped in stable phase at the end of the FEL. (Subscript 0 indicates initial conditions, tilde indicates design conditions.)

FEL design conditions									
\tilde{J} (A/cm ²)	0.1	0.32	1.0	3.2	10	32	100	320	1000
Length (m)	59	56	49	38	27	17	11	7	4
Operating parameters	Percent trapped								
Operated as designed	15	15	16	19	27	40	53	67	78
$\gamma_0 = 1.013\tilde{\gamma}_0$	8	8	8	9	10	15	25	40	65
$\gamma_0 = 0.987\tilde{\gamma}_0$	9	8	8	7	3	0	54	75	83
$\Delta\gamma = 0.75\tilde{\Delta\gamma}$	19	20	22	29	38	47	64	75	79
$\Delta\gamma = 1.25\tilde{\Delta\gamma}$	11	10	11	12	17	29	45	55	68
$I_0 = 0.5\tilde{I}_0$	8	9	9	13	22	38	49	63	74
$I_0 = 2\tilde{I}_0$	20	20	21	24	31	39	56	73	79
$B = \pm 0.015\tilde{B}$	14	14	15	17	25	39	50	65	77
$B = \pm 0.025\tilde{B}$	0.4	0.4	0.8	1.5	1.5	18	52	71	74
$J = 0.32\tilde{J}$	14	14	11	7	6	3	7	27	41
$J = 3.2\tilde{J}$	15	18	24	35	47	54	70	74	76

in Table II is the length of the amplifier for each value of the current density. An examination of this chart quickly reveals that the FEL is an inherently stable device. As current densities reach 100 A/cm² ($J_A = 41.2$ A/cm²), the only real difficulties occur when the electron energy is too high or the current density is too low. At still higher current densities, even this problem disappears. The amplifier's performance at lower current densities is noticeably degraded when either γ , $\Delta\gamma$, I , or the magnetic field profile is altered. These results point to the advantages of high current density operation [Eq. (35)] of FEL amplifiers.

Table II also indicates that the FEL amplifier works well even when the input to the wiggler is allowed to fluctuate about design values. One might then be tempted to design for higher current densities than the application requires but operate at some lower value. This would result in a shorter FEL amplifier. For example, a 320-A/cm² design operated at 100 A/cm² achieves 25% deceleration in 7 meters instead of the 11 meters called for by the 100-A/cm² design (cf. Table II). Only 27% of the electrons are trapped, however, which results in lower efficiency. One might be willing to sacrifice efficiency for length, but, unfortunately, this results in a device with greatly reduced stability. This amplifier does not work at all (no electrons remaining trapped after 25% deceleration) if the initial electron energy is too low [$\gamma(0) = \tilde{\gamma}(0) - \Delta\gamma$], or the energy spread is too large ($\Delta\gamma = 1.25\Delta\tilde{\gamma}$). If the energy is too high [$\gamma(0) = \tilde{\gamma}(0) + \Delta\gamma$], only 15% of the electrons remain trapped. Once again, one might be willing to sacrifice some stability if the amplifier can be made shorter.

Finally we note that although Table II was constructed for constant-phase-angle deceleration designs, there are circumstances (high current density) under which the programmed bucket-growth designs perform even better. For example, if we design an FEL which duplicates Fig. 2 for the first 7.5 meters and then switches to a programmed bucket-deceleration design to prevent the bucket from shrinking, we find 61% of the electrons still trapped after 11.5 meters and a 25% deceleration. This compares to 53% trapped after 11 meters of the standard design.

V. CONCLUSIONS

We have examined several different configurations of the FEL amplifier. In all the designs examined, high current density increased the amplifier efficiency and led to increased stability. We found that careful bucket control led to higher trapping fractions, but that there was a limit to the amount of energy which could be extracted from the electron beam in the tapered-wiggler FEL before electrons were lost from a full bucket. Generally, one can trade amplifier gain for increased stability, but in devices with commercial applications, this might not be desirable.

ACKNOWLEDGMENTS

The authors would like to thank H. Haus, N. Kroll, P. Morton, and L. Schlitt for suggestions which aided this work. This work was performed under the auspices of the U. S. Department of Energy by Lawrence Livermore National Laboratory under Contract No. W-7405-ENG-48.

¹H. Motz, *J. Appl. Phys.* **22**, 524 (1951).

²D. A. G. Deacon, L. R. Elias, J. M. J. Madey, G. J. Ramian, H. A. Schwettman, and T. I. Smith, *Phys. Rev. Lett.* **38**, 892 (1977).

³D. M. McDermott, T. C. Marshall, S. P. Schlesinger, R. K. Parker, and V. L. Granatstein, *Phys. Rev. Lett.* **41**, 1368 (1978).

⁴T. Kwan, J. M. Dawson, and A. T. Lin, *Phys. Fluids* **20**, 581 (1977).

⁵T. Kwan and J. M. Dawson, *Phys. Fluids* **22**, 1089 (1979).

⁶N. M. Kroll, P. L. Morton, and M. N. Rosenbluth, in *Free Electron Generators of Coherent Radiation*, edited by S. F. Jacobs, H. S. Pilloff, M. S. Sargent III, M. O. Scully, and R. Spitzer (Addison-Wesley, Reading, Mass., 1980), p. 89.

⁷A. Szoke, V. K. Neil, and D. Prosnitz, in *Free Electron Generators of Coherent Radiation*, edited by S. F. Jacobs, H. S. Pilloff, M. S. Sargent III, M. O. Scully, and R. Spitzer (Addison-Wesley, Reading, Mass.,

1980), p. 175.

⁸M. Sargent, M. O. Scully, and W. E. Lamb, *Laser Physics* (Addison-Wesley, Reading, Mass., 1974), p. 100.

⁹L. Schlitt and D. Prosnitz (unpublished).

¹⁰M. Stanley Livingston and John P. Blewett, *Particle Accelerators* (McGraw-Hill, New York, 1962), Chap. 9, p. 637.

¹¹D. Prosnitz and A. Szoke, Lawrence Livermore National Laboratory, Livermore, California, Report No. UCID-18703 (unpublished).

¹²Clearly one could choose to keep b_w/k_w^2 constant or even increasing, say, as design option (29), but this leads to a highly impractical design which results in severe transverse-field problems.

¹³The long wavelength of this FEL would require operation in an oversized waveguide.

¹⁴C. A. Brau and R. K. Cooper, in *Free Electron Generators of Coherent Radiation*, edited by S. F. Jacobs, H. S. Pilloff, M. S. Sargent III, M. O. Scully, and R. Spitzer (Addison-Wesley, Reading, Mass., 1980),

- p. 647.
- ¹⁵V. K. Neil, Jason Technical Report No. JSR-79-10
(SRI Int.) (unpublished).
- ¹⁶N. M. Kroll and M. N. Rosenbluth, in *Free Electron*

Generators of Coherent Radiation, edited by S. F. Jacobs, H. S. Pilloff, M. S. Sargent III, M. O. Scully, and R. Spitzer (Addison-Wesley, Reading, Mass., 1980), p. 147.